Science of the Total Environment 947 (2024) 174378

Contents lists available at ScienceDirect

Science of the Total Environment

journal homepage: www.elsevier.com/locate/scitotenv

Rainfall seasonality dominates critical precipitation threshold for the Amazon forest in the LPJmL vegetation model

Da Nian [a,*], Sebastian Bathiany [a,b], Boris Sakschewski [a], Markus Drüke [a,c], Lana Blaschke [a,b], Maya Ben-Yami [a,b], Werner von Bloh [a], Niklas Boers [a,b,d]

[a] Potsdam Institute for Climate Impact Research, 14473 Potsdam, Germany
[b] Earth System Modelling, School of Engineering and Design, Technical University Munich., Munich 80333, Germany
[c] Deutscher Wetterdienst, Hydrometeorologie, Frankfurter Str., 135, 63067 Offenbach, Germany
[d] Department of Mathematics and Global Systems Institute, University of Exeter, Exeter EX4 4QF, UK

HIGHLIGHTS

- In simulations of the Amazon rainforest, we find a critical precipitation threshold below which biomass decreases rapidly.
- Crossing the threshold is reversible when increasing precipitation again.
- Significant "early warning signs" can be detected before the critical threshold.
- We attribute spatial differences of the critical threshold to (i) the precipitation seasonality, (ii) potential evapotranspiration, (iii) the role of adaptive deep roots in regions with larger water stress.

GRAPHICAL ABSTRACT

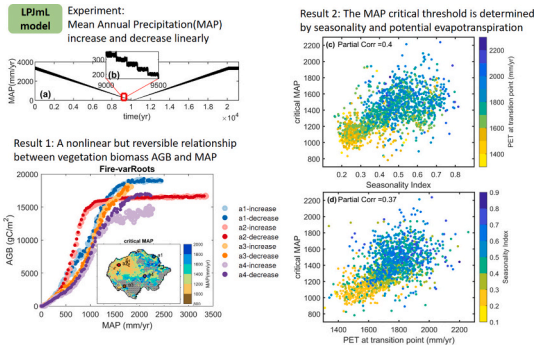

ARTICLE INFO

Editor: Jurgen Mahlknecht

Keywords:
Amazon forest
Critical precipitation
Tipping points
LPJmL model
Alternative stable states
Forest drought resistance
Climate change

ABSTRACT

Understanding the Amazon Rainforest's response to shifts in precipitation is paramount with regard to its sensitivity to climate change and deforestation. Studies using Dynamic Global Vegetation Models (DGVMs) typically only explore a range of socio-economically plausible pathways. In this study, we applied the state-of-the-art DGVM LPJmL to simulate the Amazon forest's response under idealized scenarios where precipitation is linearly decreased and subsequently increased between current levels and zero. Our results indicate a nonlinear but reversible relationship between vegetation Above Ground Biomass (AGB) and Mean Annual Precipitation (MAP), suggesting a threshold at a critical MAP value, below which vegetation biomass decline accelerates with decreasing MAP. We find that approaching this critical threshold is accompanied by critical slowing down, which can hence be expected to warn of accelerating biomass decline with decreasing rainfall. The critical precipitation threshold is lowest in the northwestern Amazon, whereas the eastern and southern regions may already be below their critical MAP thresholds. Overall, we identify the seasonality of precipitation and the potential evapotranspiration (PET) as the most important parameters determining the threshold value. While vegetation fires show little effect on the critical threshold and the biomass pattern in general, the ability of trees to adapt to water stress by investing in deep roots leads to increased biomass and a lower critical threshold

* Corresponding author.
E-mail address: danian@pik-potsdam.de (D. Nian).

https://doi.org/10.1016/j.scitotenv.2024.174378
Received 4 December 2023; Received in revised form 20 June 2024; Accepted 27 June 2024
Available online 1 July 2024

in some areas in the eastern and southern Amazon where seasonality and PET are high. Our findings underscore the risk of Amazon forest degradation due to changes in the water cycle, and imply that regions that are currently characterized by higher water availability may exhibit heightened vulnerability to future drying.

1. Introduction

As the largest tropical forest on Earth, the Amazon rainforest is a key component of the Earth system (Nobre et al., 2021; Verweij et al., 2009; Flores et al., 2024). However, this rainforest is under threat from deforestation (Lovejoy and Nobre, 2019; Lapola et al., 2023; Boers et al., 2017), climate change (Nobre et al., 2021; Armstrong McKay et al., 2022; Drijfhout et al., 2015; Wunderling et al., 2021a, 2023; Canadell et al., 2021), and the physiological forcing of increasing CO_2 (Langenbrunner et al., 2019; Richardson et al., 2018).

A large body of research indicates that tropical forests, and the Amazon in particular, may have multiple stable equilibrium states and could abruptly and irreversibly transition between these states at bifurcation points, where the mean annual precipitation falls below a critical threshold (Lenton, 2011; Staver et al., 2011; Lenton et al., 2008; Lovejoy and Nobre, 2018; Hirota et al., 2011; Staal et al., 2020; Ciemer et al., 2019; Boulton et al., 2022). Since the Amazon hosts a large fraction of the world's species and large stocks of terrestrial carbon, it is crucial to understand the mechanisms that may lead to the existence of multiple tree cover modes in the Amazon, and how these mechanisms might cause accelerated and possibly irreversible forest loss (Malhi et al., 2009; Verweij et al., 2009; Lenton et al., 2019; Smith et al., 2022; Drüke et al., 2023; Bultan et al., 2022).

The bifurcation hypothesis assumes that effectively the entire regional vegetation system can be conceptualized as a low-dimensional model. When focusing on small-scale processes such as vegetation fires, the assumption of space-for-time substitution (Hirota et al., 2011; Staver et al., 2011) implies that different sites can be understood as realizations of that same system. Large-scale feedbacks between rainfall and vegetation, for instance those related to moisture recycling (Zemp et al., 2017), have also been invoked to argue for the potential existence of feedback-driven tipping points, in which case the low-dimensional model would represent the entire Amazon as one uniform system. In both cases, the argument relies on a nonlinear response of vegetation to changes in mean annual precipitation (MAP) as an environmental control parameter (Ahlström et al., 2017). However, even without any feedback mechanisms that may give rise to a bifurcation, the Amazon could still have a reversible nonlinear response to climate change. Even such a reversible response would have severe impacts, for example on regional climate and the global carbon cycle.

Few studies have used dynamic global vegetation models (DGVMs) directly to investigate whether vegetation actually follows a nonlinear response to gradual precipitation changes. Additionally, the applicability of bifurcation theory to the extensive spatial scale of the Amazon forest tree cover remains unknown. When using the theory of bifurcation-induced tipping points to study Amazon vegetation resilience, studies assume that tropical forests have a somewhat universal critical MAP (Staal et al., 2020; Wunderling et al., 2021b). However, satellite observations indicate that forests in various locations may have different critical thresholds (Tirabassi and Masoller, 2023; Valencia et al., 2024).

At the same time, previous studies have used bifurcation theory and observational data to suggest that the Amazon forest is losing resilience, and may even be approaching a critical transition (Boulton et al., 2022; Smith et al., 2022; Blaschke et al., 2023). Resilience in this case is defined as the ability of the vegetation system to recover from perturbations such as drought and fires (Dakos and Kéfi, 2022; Buxton et al., 2022). Understanding the factors that influence vegetation resilience is crucial in defining our current safe operating space. However, the drivers and mechanisms behind the observed vegetation resilience changes remain elusive. The main concerns with regard to the future resilience of the Amazon rainforest are: the decrease in available soil water due to increased potential evapotranspiration (Brauman et al., 2012), a prolonged dry season (Fu et al., 2013), and the reduced moisture recycling resulting from the stomatal closure induced by CO_2 concentrations (Richardson et al., 2018), fires (Drüke et al., 2023), deforestation (Lovejoy and Nobre, 2019) and temperature stress and thermal maxima of physiological processes (Christopher et al., 2023). Smith and Boers (2023a) analyzed the restoring rate from perturbations in tropical forests, and showed that water availability and variability are important factors for driving resilience change. It has also been shown that different tree rooting strategies affect the dominance of tree species in South America (Sakschewski et al., 2021), which can have implications for the adaptive capacity of the rainforest to long-term climate change. While simple conceptional models can neither include so many factors at play nor represent spatial differences, these aspects are represented in DGVMs. Many DGVMs are able to simulate the distribution and dynamics of vegetation when driven by atmospheric variables such as precipitation and temperature (Sitch et al., 2008; Sakschewski et al., 2021; Drüke et al., 2021a; Gouttevin et al., 2012). These models also project the potential impacts of climate change on forests based on potential future climatic scenarios (Malhi et al., 2009; Parry et al., 2022; Cox et al., 2004).

DGVMs are hence a valuable tool to evaluate if low-dimensional bifurcations and tipping points are a plausible feature of the Amazon forest on a large spatial scale. In this study, we use the DGVM Lund-Potsdam-Jena managed Land (LPJmL) model to simulate the vegetation response to precipitation change over the Amazon basin (see Methods). By using the model offline (uncoupled to the atmosphere) we focus on the vegetation's response to climate change, but do not consider any interactions between atmosphere and vegetation. In other words, we here explore the small-scale hypothesis (similar to Hirota et al. (2011) and Staver et al. (2011)), but not the question of a potential hysteresis in the large-scale coupled dynamics of the Earth system.

The LPJmL 4.0 model (Sitch et al., 2003; Schaphoff et al., 2018a) serves as a well-established and rigorously validated process-based vegetation model. Schaphoff et al. (2018b) evaluated LPJmL4 using in situ measurements, satellite observations, and agricultural yield statistics, demonstrating its strong performance in reproducing carbon fluxes, particularly global NBP and local NEE, and showing LPJmL4 suitable for process-based analyses of biosphere dynamics and multi-sectoral climate change impacts. It comprehensively simulates the surface energy balance, water fluxes, carbon fluxes, and stocks, and the dynamics of natural and managed vegetation across the globe, driven by climate and soil input data. We conduct two primary experiments for each model configuration: the "decrease experiment", which gradually reduces precipitation from current-day levels to zero, and the "increase experiment", which restores precipitation back to its contemporary state by reversing the decrease experiment in time. This allows us to study the effect of varying MAP on the simulated Amazon forest's above-ground biomass. As local water availability is also influenced by rainfall seasonality and the loss of soil water via evapotranspiration, we investigate the role of MAP, seasonality indices, and potential evapotranspiration (PET). We also explore the role of fire feedbacks and local forest adaptation via deep rooting strategies (Sakschewski et al., 2021), by enabling and disabling different modules: (i) LPJmL with variable tree rooting strategies (parameterized as different maximum root depths, see Nepstad et al. (1994); Oliveira et al. (2005); Sakschewski et al. (2021)), (ii) LPJmL with interactive vegetation fires as simulated by the SPITFIRE fire module (Thonicke et al., 2010; Drüke et al., 2019). In the following

Methods section, we provide a detailed description of the specific settings and configurations used in our models.

2. Methods

2.1. Experiment design and setting

We here use the DGVM LPJmL4.0 (Schaphoff et al., 2018a) with disabled land use. LPJmL depicts global vegetation distribution through the fractional coverage of distinct plant functional types (PFTs), quantified as foliage projective cover (FPC). Additionally, managed land is represented through the fractional coverage of crop functional types (CFTs). Bioclimatic constraints and the influences of factors such as heat, productivity, and fire on plant mortality determine the establishment and persistence of various PFTs. This feature empowers LPJmL to unravel intricate feedback mechanisms, including those between vegetation and fire and between roots and water availability. Since its original implementation by Sitch et al. (2003), LPJmL has undergone continuous refinement. Notable improvements include the incorporation of a water balance representation (Gerten et al., 2004), an agriculture module (Bondeau et al., 2007), novel components dedicated to fire dynamics (Thonicke et al., 2010; Drüke et al., 2019), permafrost interactions (Schaphoff et al., 2013), and phenology (Forkel et al., 2019). These enhancements collectively augment the model's capacity to capture and simulate the complex interactions within the Earth's system, amplifying its utility in addressing intricate research questions. In this study, the LPJmL version we apply does not include nutrient limitations like nitrogen or phosphorus. In its standard configuration, consistent with our study, the model operates on a latitude-longitude grid, encompassing a spin-up period of 5000 years. During this spin-up phase, the model replicates the initial 30 years of the provided climate dataset to ensure convergence and stability.

We refer to the LPJmL4.0 model with variable roots (LPJmL4.0-VR) (Sakschewski et al., 2021) and the LPJmL4.0 model with the SPITFIRE module (LPJmL4.0-SPITFIRE) (Drüke et al., 2019), using the coupled LPJmL4.0 model with variable root module and SPITFIRE module (LPJmL4.0-VR-SPITFIRE) to mimic the dynamical vegetation responses under precipitation control over Amazon rainforest region. We first study the effect of plant root depths strategy by comparing a model version with fixed maximum root depth to a version where maximum root depth is dynamic (Sakschewski et al., 2021) and can reach down to the total soil depth (which differs spatially). While in principle, two tropical tree types exist in LPJmL, enabling variable roots results in 20 natural tropical tree types with different maximum root depths. The second effect, the role of wildfires, is studied by enabling the SPITFIRE module (Drüke et al., 2019; Thonicke et al., 2010). SPITFIRE is a process-based fire model, which simulates danger, ignition, spread, and effects of fire coupled to the vegetation dynamics in LPJmL. By enabling or disabling the deep variable root and SPITFIRE modules, four model versions were assessed: wildfire with deep root influence (Fire-varRoots), wildfire without deep root influence (Fire-fixedRoots), no wildfire with variable root influence (noFire-varRoots), and no wildfire without variable root influence (noFire-fixedRoots). CO_2 levels are kept constant at pre-industrial levels, and no land use is imposed in order to be able to focus on the effect of the factors described above.

To assess if the vegetation system in the LPJmL model demonstrates a nonlinear and irreversible response consistent with bifurcation theory, it is essential to examine how vegetation biomass responds to changes in precipitation. The most straightforward method involves linearly reducing precipitation to zero and then incrementally restoring it to its original level, observing the vegetation response throughout. To investigate the impact of precipitation on the equilibrium state of the vegetation system, the precipitation is slowly decreased from the long-term observational climatology of the Amazon region to zero, and then increased to its original level. The input climatology is based on 1981–2010 climate observations from CRU TS v. 4.06 (Climatic Research Unit gridded Time Series) dataset (Harris et al., 2020). In the experimental design, precipitation levels for each grid cell were modulated. This is implemented in the precipitation-decreasing experiment through a gradual reduction from current levels to zero, at a rate of 1 % per 100 years. Conversely, in the precipitation-increasing experiment, the increase is gradual from zero back to the original levels, maintaining the same rate. The precipitation change is executed in a step-like manner: Every hundred years, we decrease (or increase) precipitation by 1 % of the initial value at the first year and continue to run for 99 years to ensure the system is in equilibrium or quasi-equilibrium, while all other climate forcings are kept constant. While the scaling factor to achieve this reduction drops from 1 to 0 in a step-wise fashion, precipitation can still fluctuate from year to year due to natural variability (see Fig. 1a, b), which was simulated by adding the randomized shuffling of 1981–2010 climate data. This shuffling process introduces the interannual variability in the experiment. Since the experiment only uses the climatological variability between 1981 and 2010 with a shuffling procedure, its impact on vegetation does not reflect the full interannual variability in the real climate, and so it will not be discussed in detail here. To bring the vegetation into equilibrium after the ramp-up, we also ran the model for another 1000 years at constant original precipitation levels after the precipitation finally returned to present-day levels (Fig. 1a). The length of the MAP and AGB time series spans 10,100 years for the decrease experiment and 11,100 years for the increase experiment, with the range of MAP values varying across grid cells.

To analyze the relationship between MAP and AGB, we initially smooth and filter the MAP and AGB to eliminate high-frequency signals below 100 years by filtering using a 2th-order lowpass digital Butterworth filter (Mitra, 2001), which is caused by the discontinuous precipitation changes of 1 % every 100 years (Fig. 1b). We then establish a rescaled MAP time series with a consistent interval of 25 mm/yr, ranging from 0 to its maximum, and identify the corresponding AGB value for each MAP to derive the new rescaled AGB for each grid cell. This process ensures that the rescaled MAP of all grid cells start at zero and have the same interval, enabling a more convenient comparison of the rescaled AGB across different grid cells at the same MAP despite different data length. We use the relation between the rescaled MAP and AGB to identify the critical MAP and for classification via the unsupervised Self-Organizing Map (SOM) method (Vatanen et al., 2015). Based on the experience of many attempts, we chose to divide into 8 clusters. The number of clusters has little effect on the resulting pattern.

2.2. Determining critical MAP and water availability indices

To determine the critical MAP in a consistent manner, we employ a conditional average of three methods. (1) For the first method, a single change point detection technique is used. It selects a point to divide the signal into two parts and computes the error sum of squares between each signal part and the linear least-squares fit for that part as a residual error. The location of the division point is adjusted until the total residual error is minimized. This transition point detection method is implemented using the 'findchangepts' function in Matlab2021b (MATLAB, 2021). (2) The second method also uses a change point detection approach but includes a threshold for minimum improvement in total residual error set to 10^6. This method may identify more than one change point and operates similarly to the first method, but it continues to find additional change points until the total residual error is first below the defined threshold. The transition point is determined as the change point with the max slope differences between the two sections before and after it. This method is implemented using the 'findchangepts' function in Matlab2021b (MATLAB, 2021). (3) The third method estimates the point of maximum curvature by the derivative method. The curvature K can be estimated as follows:

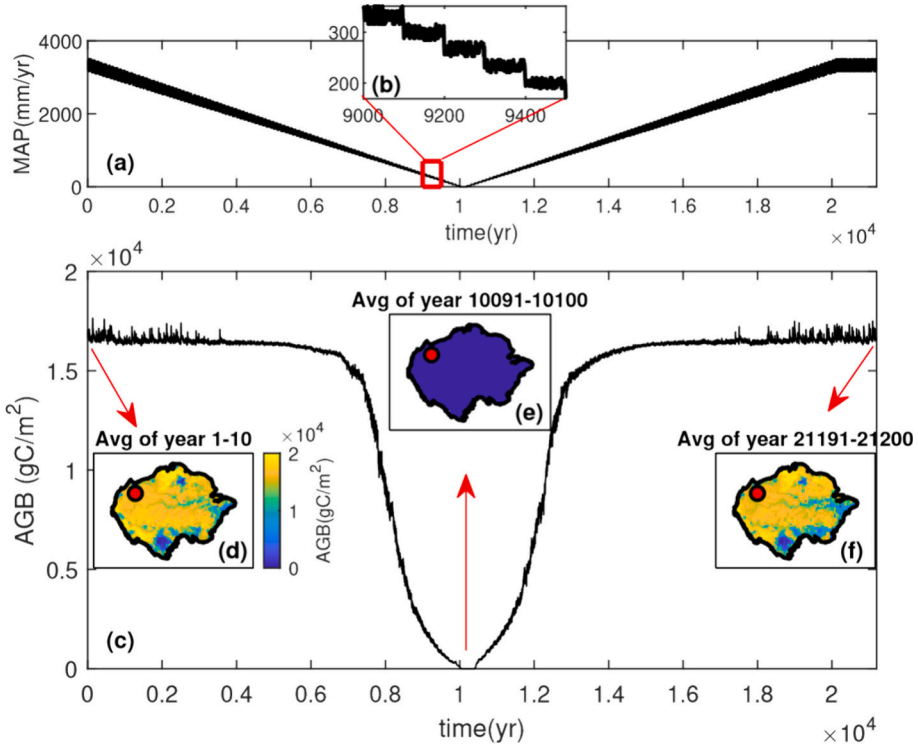

Fig. 1. Design of the precipitation control experiment using the LPJmL model. (a) Illustrates the gradual reduction of precipitation from current levels to zero at a rate of 1 % per 100 years, and its subsequent rise back to original levels at the same pace. This precipitation level then remains for an additional 1000 years to ensure equilibrium at the end. (b) shows each 100-year change is executed by reducing by 1 % of the initial value in the first year and maintaining this level for the following 99 years. This process also incorporates interannual variability by shuffling 1981–2010 climate data. (c) Showcases the progression of Above Ground Biomass (AGB) at a chosen grid cell (the red dot in (d)) during the precipitation control experiment. (d), (e), and (f) Display the time-averaged AGB patterns in the Amazon during the initial state (years 1–10), at zero precipitation (years 10,091–10,100), and after the restoration to initial precipitation levels (years 21,191–21,200). The Amazon basin is determined from (http://worldmap.harvard.edu/data/geonode:amapoly ivb).

$$K = \frac{|y''|}{(1+y'^2)^{\frac{3}{2}}} \quad (1)$$

where the AGB is a function of MAP, denoted by y. y' represents the first derivative$y' = \frac{dAGB}{dMAP}$, and y'' represents corresponding second derivative. The difference between the slopes of the sections split at the maximum curvature point is calculated. In order to circumvent potential inaccuracies in transition point detection due to high-curvature local fluctuations, the calculation process is repeated for each point with decreasing curvature values, from the maximum down to the point of 1/3 maximum curvature. The point showcasing the largest positive slope difference is designated as the transition point. The critical MAP threshold in this study is then computed as a conditional average of these three methods' results. If a result varies from the other two by >1000 mm/yr, it is considered an outlier and excluded from the average calculation, e.g. Supplementary Fig. A1. If any of these three methods fail to determine the critical threshold, we consider the corresponding critical MAP at that grid cell as indeterminate.

To further explore the factors influencing critical MAP, we focus on the importance of water availability. Since local water availability is affected by rainfall seasonality, we examine the role of seasonality. Given that precipitation is prescribed in the experiment, simple seasonal variability metrics, e.g. the standard deviation of monthly precipitation in each year, would be biased by the absolute MAP, meaning the variability metrics would change with controlled MAP. To mitigate the influence of absolute MAP, we refer to Walsh-Lawler Seasonality Index (Walsh and Lawler, 1981) as the measure of precipitation seasonal variability metrics, which excludes the absolute value influence:

$$SI = \frac{1}{R}\sum_{n=1}^{n=12}|x_n - R/12| \quad (2)$$

in where R is the mean annual precipitation, x_n is mean rainfall of month n.

The aridity index is estimated by MAP relative to potential evapotranspiration (PET). The dry season precipitation (DSP) is determined by first calculating the 3-month running mean over the entire period and then selecting the minimum value of each year as dry season precipitation, which refers to the same method in Chou et al. (2013).

To explore the relationship between critical MAP and other variables, we also calculate the aridity at the critical MAP value, and analyze the relationship between aridity and AGB under varying SI levels. We use partial correlation to estimate the linear partial correlation coefficients between two variables among three variables controlling for the third variable. This can be achieved directly by 'partialcorr' function in Matlab 2021b (MATLAB, 2021).

2.3. Dynamical system early warning indicators

When a stable state described by a dynamical system loses stability (or resilience, in the sense of recovery rate; see Holling (1973); Pimm (1984); Held and Kleinen (2004); Boers (2021); Brovkin et al. (2021)), it is known to show so-called Critical Slowing Down (CSD) (Scheffer et al., 2009; Lenton, 2011; Boers et al., 2022). CSD indicators like the autocorrelation and the variance are hence commonly used as early warning indicators for critical transitions (Dakos et al., 2008). Specifically, in a stochastic dynamical system with a bifurcation point (where the current stable state is lost), the temporal variance and lag-1 autocorrelation (AR (1)) coefficient will increase as the control parameter approaches this

point (Scheffer et al., 2009).

Based on this theory, assuming that the dynamics are close to the equilibrium, linearize the system around a fixed stable point x^* for the fluctuations $\Delta x = x - x^*$:

$$d\Delta x = \lambda \Delta x dt + \sigma dW \tag{3}$$

which defines an Ornstein–Uhlenbeck process a Wiener Process W and standard deviation σ. The fixed point is stable for restoring rate $\lambda < 0$. Discretizing this process into a time step Δt, the variance and AR(1) are obtained via Dijkstra (2013):

$$\langle \Delta x^2 \rangle = \frac{\sigma^2}{1 - e^{2\lambda \Delta t}} \tag{4}$$

and

$$\alpha(n) = e^{n\lambda \Delta t} \tag{5}$$

Therefore, as the system loses stability, λ approaching zero, AR(1) (that is $\alpha(1)$) will increase toward 1 and variance $\langle \Delta x^2 \rangle$ will diverge to positive infinity, which thus can be used as precursor signals to detect critical slowing down and measure the drought resistance change of the system. To estimate the temporal variance and AR(1), we use a sliding window with a window size of 100 years. The Kendall τ patterns show the tendency of variance and AR(1) over time approaching transition points. The significance of the Kendall τ is detected by generating 100 groups of Phase-Randomized Surrogate (PRS) time series for each grid cell, and calculating their Kendall τ (Dakos et al., 2008; Nian and Fu, 2019). Kendall τ values above the 95 % percentile of the surrogate statistics are considered significant (equivalent to $p < 0.05$).

3. Results

3.1. Nonlinear response without large-scale hysteresis

The above-ground vegetation biomass generated by the model under the Fire-varRoots version is shown in Fig. 1(c,d). This version of LPJmL is able to simulate the biomass distribution and distribution of tree types fairly realistically (Fig. 1c) (Sakschewski et al., 2021).

In the decrease experiment, the AGB of Amazon forest vegetation shows initial stability as the rainfall declines gradually. However, a transition to a quasilinear regime is observed when annual mean precipitation decreases past a certain critical threshold (in the following: critical MAP), below which the forest biomass declines in response to the precipitation decrease (Fig. 1c). Observations of the Amazon forest-savanna landscape have also shown sharp transitions between two vegetation types when precipitation is varied (Tirabassi and Masoller, 2023; Valencia et al., 2024). The overall shape of linearly increasing biomass with increasing MAP and a plateau thereafter is identical in all model versions (Fig. A2). The fact that a saturation level exists can be explained by the limitation of space (imposed in the model by a maximum foliage projected cover), light, and the maximum height of trees. Due to these limitations, there is a point at which no further increase in carbon storage can be realized, even without water limitation.

In order to further analyze what determines the shape and threshold value in the nonlinear response of vegetation to precipitation, we selected four representative grid points: grid cell a2 with abundant annual precipitation (MAP>3000 mm/year); grid cell a1 with relatively high precipitation (MAP>2000 mm/year); grid cell a3 with relatively low precipitation (MAP < 2000 mm/year); and grid cell a4 which shows hysteresis. We show the changes in biomass vs precipitation at these four representative grid cells (Fig. 2). While some grid cells within the forest maintain stable high biomass levels under high MAP conditions, biomass rapidly declines to zero when precipitation falls below a critical threshold. For example, in the precipitation decrease experiment, grid cell a1 has a critical MAP of 1575 mm/year, and grid cell a2 has a critical MAP of 1025 mm/year. Above these critical MAP values, AGB remains nearly unchanged. However, when MAP drops below the critical thresholds, the rate of AGB decline is 12.9 ± 0.4 gC/m^2/mm for grid cell a1 and 17.4 ± 1.6 gC/m^2/mm for grid cell a2 (Fig. 2). In contrast, certain grid cells, such as grid cell a3, exhibit a more gradual biomass

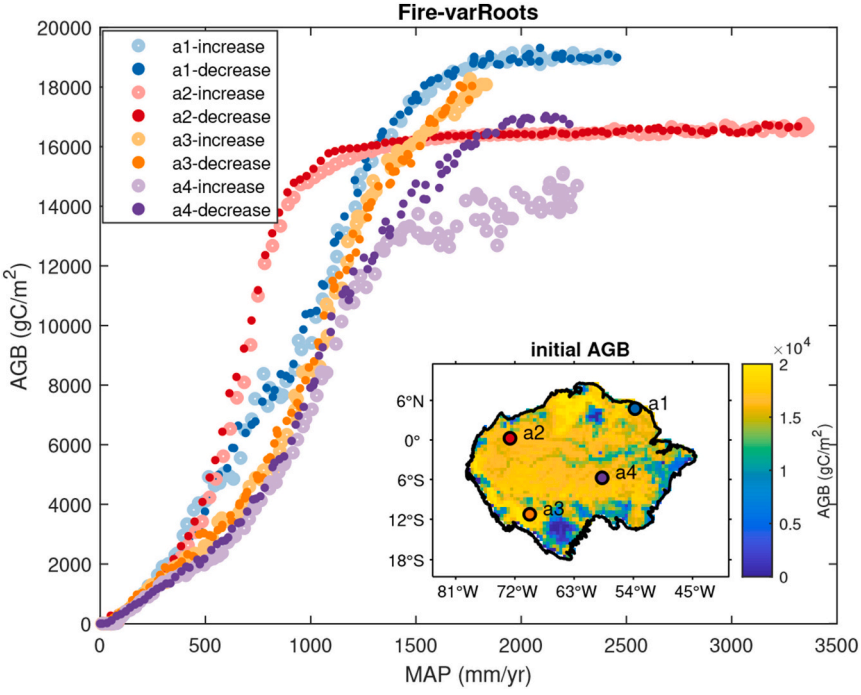

Fig. 2. Variations in Above Ground Biomass (AGB) during Mean Annual Precipitation (MAP) increase and decrease experiments at four selected Amazon forest grid cells in the Fire-varRoots version. The inset illustrates the initial AGB from climatology across the Amazon forest and the positions of the chosen grid cells. a1 locates at 4.75°N, 53.75°W; a2 at 0.25°N, 72.75°W; a3 at 11.25°S, 69.75°W; a4 at 5.75°S, 58.75°W. The MAP and AGB have been filtered to remove high-frequency signals under 100 years (see Methods), and for clearer visualization, data points are displayed at 100-year intervals.

shift in response to precipitation changes, without any abrupt changes in sensitivity. Grid cell a3 with an indeterminate critical MAP shows a slower AGB change rate of 11.7 ± 0.4 gC/m^2/mm in the precipitation decrease experiment. Often, however, the currently observed MAP at these grid points is already relatively low, so the relationship between biomass change and higher MAP is uncertain there.

Regardless of the presence or absence of a critical threshold, the trajectories of biomass change in response to precipitation during the decrease and increase experiments exhibit an almost complete overlap in all four model versions (Fire-varRoots, Fire-fixedRoots, noFire-varRoots, noFire-fixedRoots) (Supplementary Fig. A2). Also, comparing the biomass patterns at the beginning of the decrease experiment and the end of the increase experiment reveals that the overall vegetation is able to fully recover (Fig. 1d-f). In other words, we generally find no large-scale hysteresis and no alternative stable states in the model. Interestingly, there are exceptions at some grid cells (see purple grid cell a4 in Fig. 2 and Supplementary Fig. A2a,c). When comparing the AGB difference between the end of the increase experiment and the start of the decrease experiment for each model version, the Fire-varRoots model version shows that the AGB cannot recover to the same level as it was at the start of the decrease experiment in some eastern and southern regions of the Amazon (Fig. A3a). Compared to the model version without variable-root (Fig. A3b, c) and fire impacts (Fig. A3c, d), in the Fire-varRoots model more regions in the Amazon area fail to recover or exceed their previous AGB levels, even as the MAP recovers fully at the end of the increase experiment (Fig. A3a). However, during the stage where biomass gradually changes with MAP, the trajectories nearly coincide. We suspect that at these grid points the large internal biomass variability and the delay in vegetation recovery (Fig. A4) can explain the differences. In addition, we examined the Foliage Projective Cover (FPC) difference between the end of the increase experiment and the start of the decrease experiment for each model version for evergreen and deciduous trees respectively (Fig. A4). The analysis of the Fire-varRoots model version shows that there is a notable transition from evergreen to deciduous forests in the eastern and southern Amazon Basin (Fig. A4b). This transition is consistent with the AGB hysteresis areas shown in Fig. A3. This suggests that there can be hysteresis due to competition between different plant types involving fire and/or root adaptation (Drüke et al., 2023). It should be noted, however, that our experiments were run over a very long time span and had plenty of time to get close to equilibrium after each precipitation change.

Our results hence add to findings that observed no hysteresis under linear increases and decreases of CO_2 in the LPJmL model (Drüke et al., 2021b), but differ from those that show that fire can actually create multiple equilibria in a coupled version of LPJmL (coupled to an Earth system model) (Drüke et al., 2023) and in at least one other DGVM, JSBACH (Lasslop et al., 2016) (see Discussion and Conclusions).

In our simulations, the comparison between the Fire-fixedRoots and noFire-fixedRoots model versions shows little effect of fire on the overall non-linear response of vegetation in the experiment (Fig. A2b,d). While wildfire and vegetation root strategies do impact the amount of biomass that can be realized at a certain MAP level (see Fig. A5), they are not the main determinants of the non-linear response of forests to MAP in LPJmL.

However, as we will show below, there are spatial differences in the critical MAP. Previous research indicates that precipitation, its seasonality, PET, dry season precipitation (DSP), fire, and root depth all exert a nonlinear influence on vegetation AGB (Smith and Boers, 2023a; Malhi et al., 2009; Bush, 2017; Hutyra et al., 2005). In the following sections, we hence investigate how these drivers affect the critical MAP values.

3.2. Role of fire and deep roots for the critical MAP

The nonlinear transition in AGB sensitivity happens at different precipitation values for different locations (Fig. 2). Therefore, we identify the MAP value at which this transition happens and analyze the role of deep roots and fire in affecting this value.

To determine the critical MAP for each grid cell, we used three different methods to calculate the critical threshold and averaged their results (see methods). This enabled us to map critical MAP across the Amazon forest area in the decrease experiment. The result for the Fire-varRoots model version is shown in Fig. 3a. The northwestern region of the Amazon rainforest shows a relatively low critical MAP, whereas the eastern and southern regions display a higher critical MAP.

In our simulation setup, we assume that rainfall anomalies affect MAP whilst the rainfall seasonality remains unaffected. The critical MAP in this case thus represents the potential resistance to drought, which can also be regarded as a kind of resilience of the vegetation system (i.e. the inherent ability to remain unaffected by precipitation changes). As evident from Fig. 2, the lower the critical threshold, the smaller MAP can become before the forest biomass becomes sensitive to droughts. However, this also means that once biomass at the more resilient locations passes the critical MAP threshold, it will be at a lower MAP level and thus will then become particularly sensitive to further drying, giving rise to potentially rapid loss of carbon pools. The pattern of critical MAP (Fig. 3a) suggests that under the current-day climate, the northwestern Amazon would exhibit higher potential drought resistance. In contrast, the southern and eastern areas appear more vulnerable to MAP changes. These findings agree with the patterns of resilience to climate change identified in other studies (Hirota et al., 2011; Ciemer et al., 2021; Staal et al., 2020).

To further validate the critical MAP pattern, we employed the Self-Organizing Map (SOM) (Vatanen et al., 2015) method, which is an unbiased, unsupervised machine-learning technique for clustering high-dimensional data into a two-dimensional representation (see Methods). We use SOM to cluster the relationship between AGB and MAP for each grid cell in the Amazon, yielding eight clusters (Fig. 4). The results show a similar pattern of classification distribution compared to the spatial distribution of critical MAP (Fig. 3a). Because each cluster is comprised of time series with a similar shape, the clusters correspond to different critical MAPs. Evident across these varied clusters is the existence of a threshold, beyond which vegetation biomass decreases when MAP is reduced. One of the clusters exhibits no significant shift, which probably corresponds to an initial MAP value that is already below critical MAP (Fig. 4c). In some areas of the southern and eastern Amazon, we did not identify a critical MAP value (Fig. 3a) (see Methods). Interestingly, the regions in most southern parts where we cannot detect a critical MAP align with the regions of low climatological MAP (Fig. A6). It is therefore plausible that in these regions the vegetation at the start of the simulation is already below the critical MAP threshold. This is the case for cells in cluster 1 (Fig. 4c). Only a few grid cells in the southernmost part of the Amazon show a critical MAP, and these are also the cells with a high climatological MAP.

All four model versions (Fig. A7) demonstrate similar spatial patterns of critical MAP. One of the few differences between the model versions is that there are larger critical MAP values (>2000 mm/yr) in the southern and eastern Amazon Basin in the model with deep-root strategy. The probability density functions (PDFs) for the critical MAP of all four model versions are also similar. Minor differences indicate that in the versions with fire, the PDFs for critical MAP values tend to be broader with more distribution of large critical MAP values. Root strategy and fire disturbance are not factors in determining critical precipitation threshold patterns in most of the Amazon forest (Fig. A7), but they still play a role for the critical MAP in some areas (Fig. A8). Compared with the impact of fire disturbance on critical MAP, the impact of root strategies is more obvious in the eastern and the northernmost parts of the Amazon forest. For some of the easternmost regions, variable-deep root strategies significantly reduced critical MAP, thereby enhancing the forest's ability to withstand drought, though small local areas in the northernmost, southern, and parts of the eastern Amazon show the opposite.

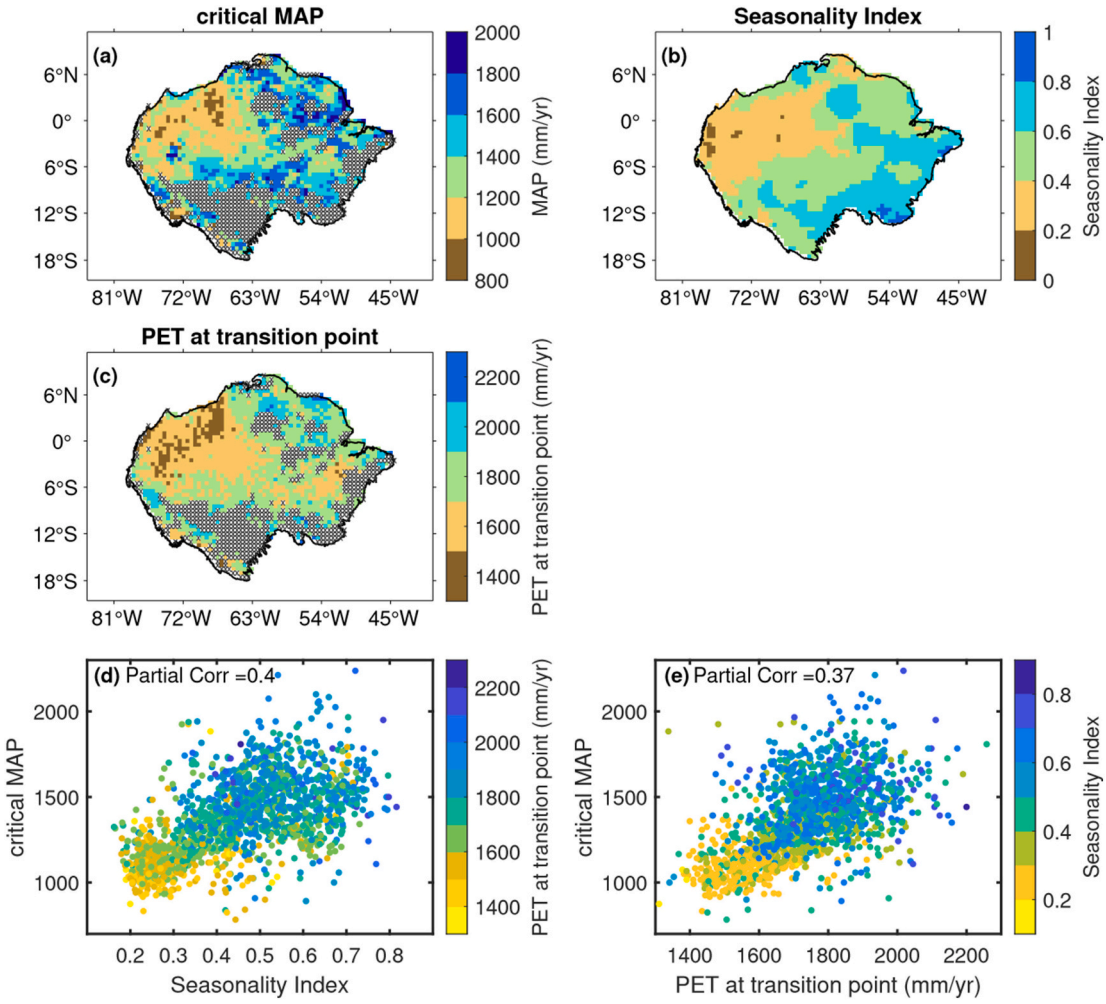

Fig. 3. The Critical MAP pattern and the relationship with other variables in the Fire-varRoots version. (a)Critical MAP pattern (the critical threshold for state transition). Hashed areas in (a) and (c) show regions where a critical threshold cannot be detected. (b)Precipitation seasonality index (SI) pattern over the Amazon. (c)The pattern of Potential Evapotranspiration (PET) at transition points over the Amazon. (d)The relationship between critical Mean Annual Precipitation (MAP) and the Seasonality Index (SI) during the precipitation-decreasing experiment. The color of each dot corresponds to the corresponding PET at transition points. The partial correlation between SI and critical MAP, given the condition of PET, is displayed in the top left corner of the subfigure. (e)The relationship between critical MAP and PET at transition points during the precipitation-decreasing experiment. The color of each dot corresponds to the corresponding SI. The partial correlation between PET and critical MAP, given the condition of SI, is displayed in the top left corner (d) and (e).

3.3. Role of seasonality and aridity for the critical MAP

The next step to understanding the non-linear characteristics of the vegetation response to MAP changes is to find out what determines the critical MAP, and why it varies in different locations. The factors which are most likely to influence the critical MAP pattern are those associated with water availability and its variability, since those have a crucial impact on the resilience of the forest (Levine et al., 2016; Smith and Boers, 2023a). Following Smith and Boers (2023a), we use precipitation seasonality, inter-annual variability, and the aridity level (long-term MAP relative to PET) as ways to quantify water variability and availability (see Methods).

We first focus on the quantitative role of rainfall seasonality, which can be expected to increase the critical MAP value: At a given MAP a larger seasonality will mean smaller rainfall in the dry season and a higher likelihood of reaching the water stress threshold, where productivity becomes limited by water (instead of radiation). Thus when MAP is gradually decreased, the threshold is reached earlier for regions with larger seasonality.

For equivalent MAP levels, larger SI values signify increased intra-annual variability in precipitation and vice versa. Large SI thus means more severe and less rainy dry seasons and implies that the vegetation experiences enhanced water stress during the dry season (Signori-Müller et al., 2021). Since the sub-annual precipitation input was scaled by the same factor within each year in our model setup, the SI is invariant in time, and is exclusively determined by the initial input of the climatology data. This allows us to separate the effect of seasonality on the critical MAP.

The results demonstrate a high spatial Pearson correlation of 0.57 between the patterns of critical MAP and SI under the Fire-varRoots version (Fig. 3 and Supplementary Fig. A7). The northwestern Amazon has a lower SI and a lower critical MAP. Conversely, the eastern and southern regions show a higher SI, because of the larger difference between the dry and wet seasons in these areas. These regions also have a higher critical MAP. A similar relation is observed across all four model versions (Supplementary Fig. A7), indicating a robust correlation between critical MAP and SI, independent of wildfire or deep-root influences. This suggests that the spatial distribution of precipitation seasonality is a key determinant of the critical MAP pattern, and the dominant factor compared to influences of fire and root strategies.

To further explore the impact of SI on the critical MAP, we examine the relationship between Above Ground Biomass (AGB) and MAP at

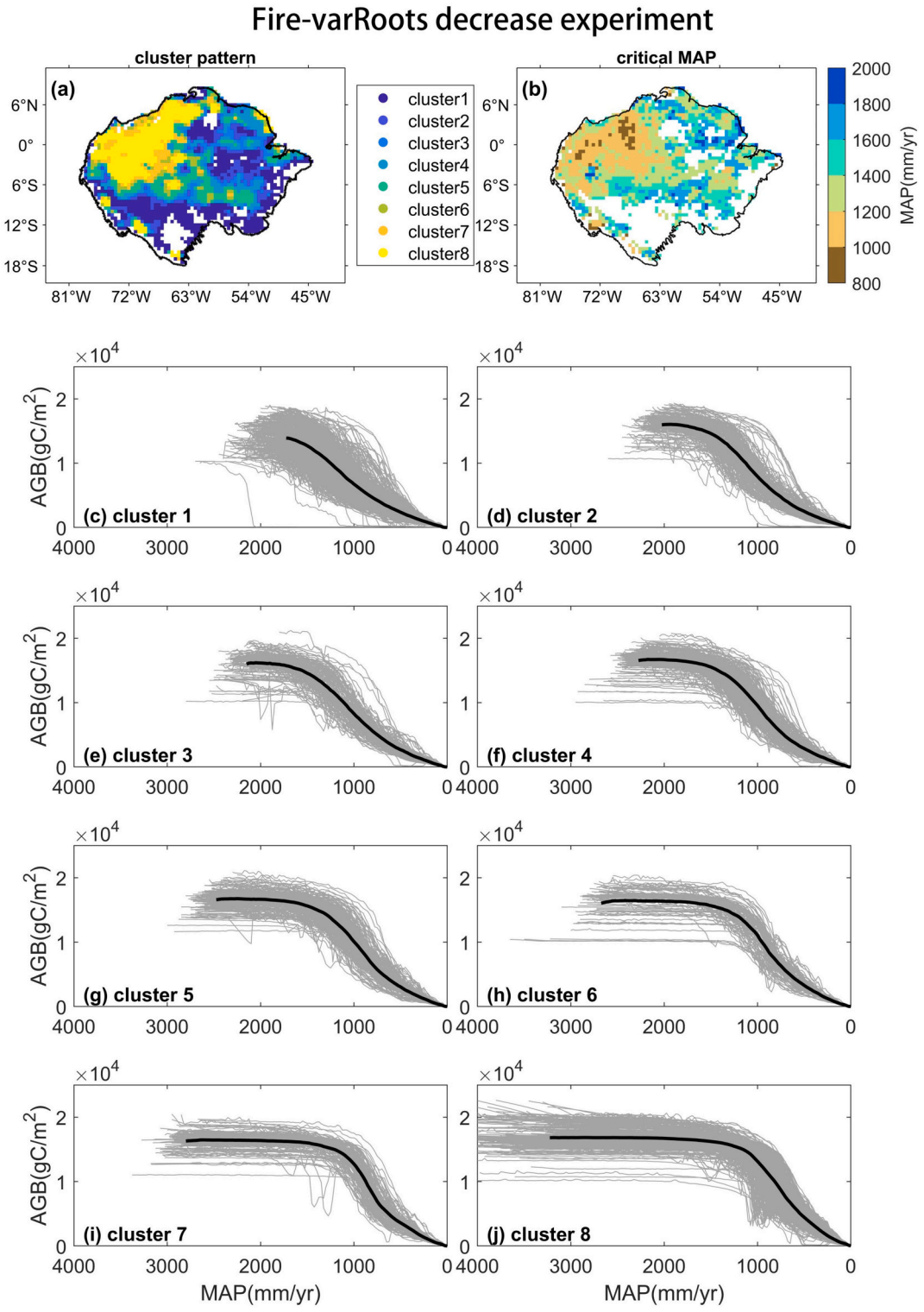

Fig. 4. Classification of the AGB variation with precipitation for the Amazon forest grid cells using the SOM method, based on the precipitation-decreasing experiment in the Fire-varRoots version. (a) Spatial distribution of all clusters by SOM classification; for easy comparison, (b) presents the pattern of critical MAP. Panels (c-j) represent the 8 clusters, where the gray line corresponds to all results assigned to each category, and the black line signifies the average value of this category (due to the different start precipitation in the decrease experiment at each grid cell, the average value can only be calculated if >70 % have values at a specific precipitation in each category). For simplicity, we consider grid points with initial AGB > 10000gC/m^2 as forests, and these grid cells are subsequently classified.

different SI values individually, for all grid cells in the Amazon during the decrease experiment. The result for the Fire-varRoots version is shown in Fig. 5, indicating that higher SI coincides with a higher critical threshold MAP.

We also examined the dry-season precipitation (DSP, see Methods) and found that the DSP pattern at the critical MAP is also correlated to

the critical MAP, though with a weaker correlation compared to the correlation between the SI and critical MAP (Fig. A9). The impact of variable-root strategies and fire disturbance, whether present or absent, overall doesn't significantly affect the DSP pattern at the critical MAP threshold (Fig. A10).

Rainfall and its distribution are, however, only a part of the moisture balance; the soil moisture available to plants also depends on runoff and evapotranspiration. An important value in this context is the aridity, which provides insight into the water availability status and offers a comparison across diverse climate and vegetation zones (Smith and Boers, 2023a). We here define aridity as PET divided by MAP.

After estimating the aridity at the critical MAP value and analyzing the relationship between aridity and AGB under varying SI levels, the results show that the aridity level at the transition point is around 1.32 for the Fire-varRoots version for all SI levels, indicating that PET is greater than precipitation and the forest is already in a water-scarce situation. The critical aridity value is similar across all four model versions (Fig. A11). This suggests that at the transition point where biomass begins to decline, grid cells at similar SI levels experience similar water availability conditions. Most importantly, we find that using aridity instead of MAP as the control variable, a larger SI still implies a larger critical MAP (Fig. 5 b, d, f, h), pointing to seasonality as a true causal explanatory variable.

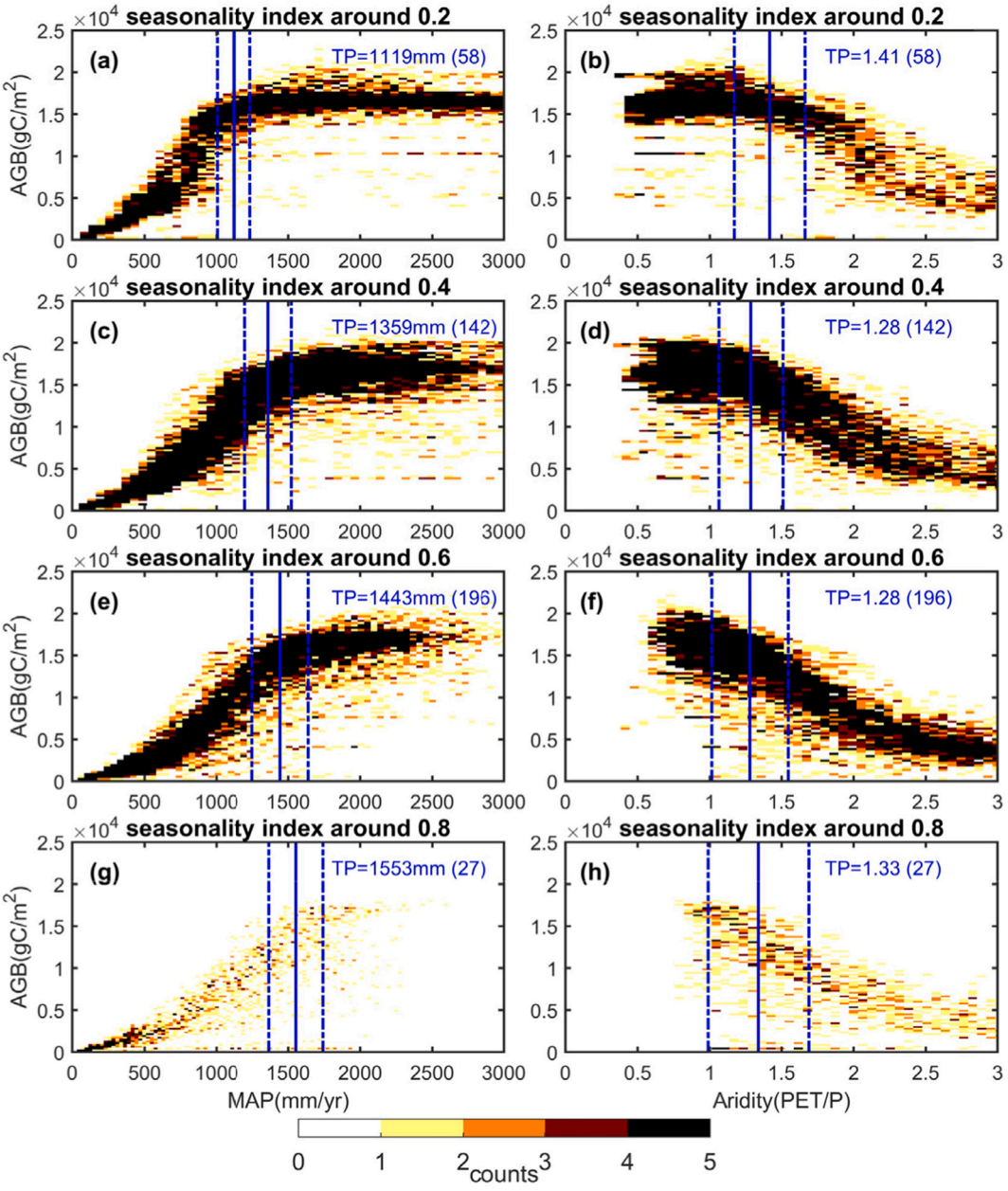

Fig. 5. Heatmap depicting the distributions of vegetation AGB under controlled precipitation and under the corresponding Aridity Index (PET/MAP) for specific SI levels in the Fire-varRoots version. The first column presents the composite distribution map between AGB and its corresponding MAP at a specific SI (a, c, e, g), while the second column shows the composite distribution map between AGB and its corresponding Aridity at a specific SI (b, d, f, h). Each row represents a different SI level, from top to bottom, corresponding to SI values of 0.2, 0.4, 0.6, and 0.8 respectively. The blue lines represent the mean critical threshold values of MAP (a, c, e, g) or Aridity (b, d, f, h) at transition points, averaged by sampling the corresponding SI levels in the range ± 0.02.'TP' means the Mean critical MAP values, which are shown in the upper right corner of each panel as blue fonts, and numbers in parentheses show sample sizes. The dashed lines indicate the range of one standard deviation around the mean. The critical MAP increases with increasing SI, whereas the Aridity remains approximately consistent around 1 at the transition point.

3.4. Early warning signals

When the CSD theory is applied to satellite observations of the Amazon forest it can be shown that tropical forests show lower resilience at locations with low MAP (Verbesselt et al., 2016; Smith and Boers, 2023a), and that large parts of the Amazon have been losing resilience in recent decades (Boulton et al., 2022). It should be emphasized, however, that great care is needed with regard to the employed vegetation index and data processing (Smith and Boers, 2023b; Smith et al., 2023).

Although the non-linear response seen in the AGB-MAP relationship in this study is not bifurcation-induced tipping, resilience may still decrease before the transition (Kéfi et al., 2013), and we can check whether CSD indicators can provide warning signals for this transition. We consequently calculate the variance and the AR(1) coefficient in sliding windows up to the critical MAP, and estimate their nonlinear trend by their Kendall τ value, where $\tau > 0$ means the trend is positive, and the larger the value, the more pronounced the increase, and vice versa (Boulton et al., 2022). In all four model versions, most grid cells exhibiting critical transitions also display gradually increasing CSD indicators, with some showing significant trends (Fig. 6). This demonstrates that CSD indicators are still partly valid for early warning signals of these critical transitions in our case, even though no bifurcation occurs. Note that the positive trends of the AR(1) coefficient and the variance are more pronounced and more significant in the experimental

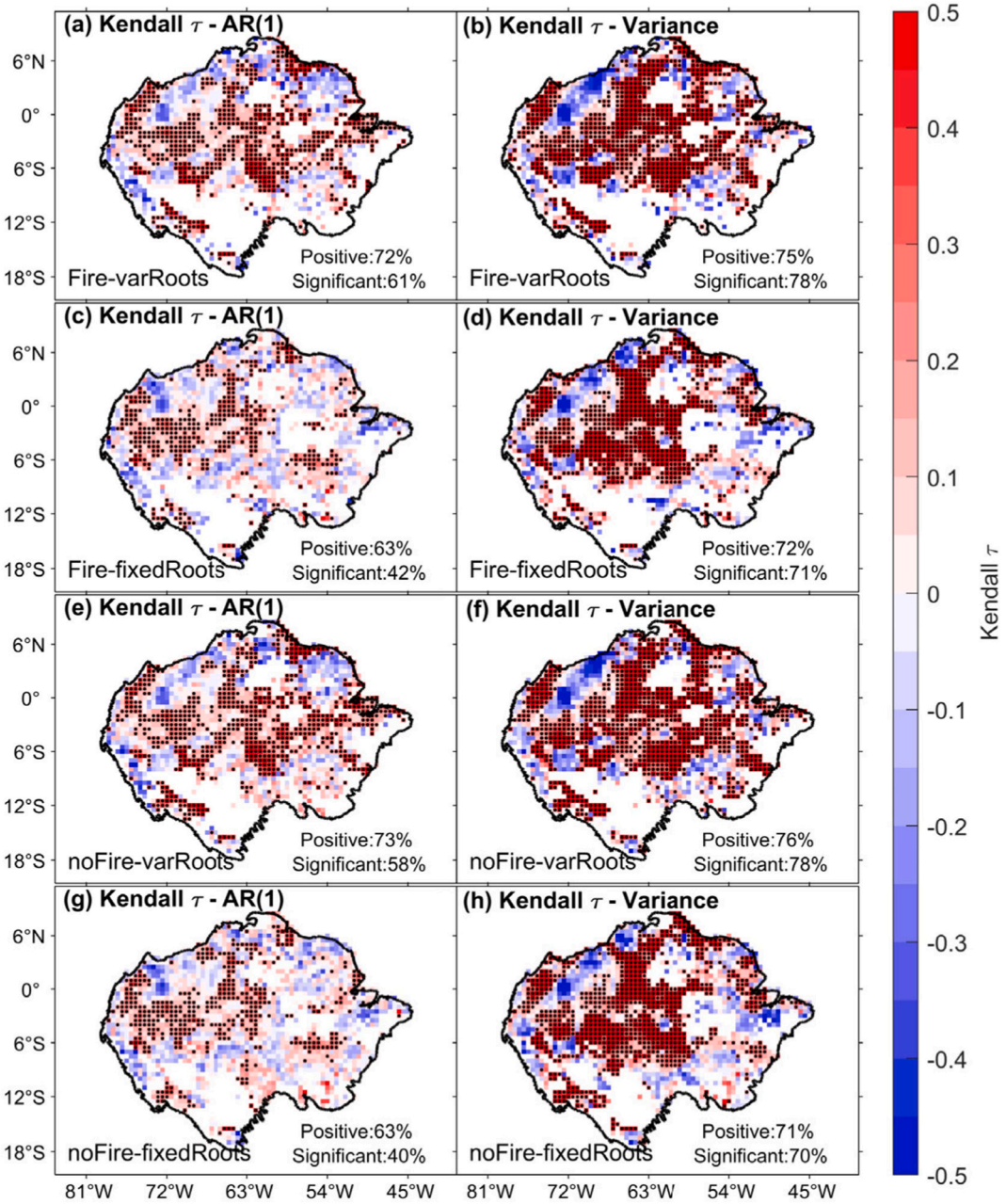

Fig. 6. Estimation of early warning indicators for Amazon vegetation prior to transitions. The first column presents maps of the Kendall τ values of AR(1) for individual grid cells before transitions (a,c,e,g). The second column displays maps of the Kendall τ values of variance for individual grid cells before transitions (b,d,f,h). Rows correspond to the Fire-varRoots, Fire-fixedRoots, noFire-varRoots, and noFire-fixedRoots version, respectively. The percentage of grid cells with positive Kendall τ for each sub-figure is indicated in the top right corner as 'Positive'. The significance of Kendall τ is evaluated using Phase-Randomized Surrogates (PRS), where a Kendall τ value is deemed significant if it surpasses 95 % of the surrogate results. The percentage of significant positive Kendall τ values out of all positive Kendall τ grid cells is indicated in the top right corner as 'Significant' for each sub-figure.

setups that consider adaptive deep roots. Additionally, when deep-root strategies are considered, the proportion of significant early warning signals is larger than in the other simulations. These patterns remain robust regardless of the sliding window size used to estimate temporal variance and AR(1), as confirmed through tests with varying window sizes shown in Supplementary Fig. A13.

4. Discussion and conclusions

We employed the advanced vegetation model LPJmL to simulate the response of the Amazon forest's vegetation system to a decrease in precipitation. The precipitation was gradually decreased to zero and then similarly returned to its original state. Our results show that in this model the vegetation AGB changes non-linearly with MAP and that a regionally varying critical MAP threshold exists below which AGB rapidly declines. In the real-world, capturing direct relationships between vegetation biomass changes and MAP variations is challenging because extreme and long-lasting changes in MAP have so far been rare. Researchers therefore employ a "space-for-time replacement" approach (Hirota et al., 2011), assuming that the biomass-MAP relationship observed across different locations reflects different stages of ecological development. The resulting distribution (Fig. A12) demonstrates a relationship similar to our simulations (Fig. 2), indicating that these simulations are credible.

This non-linear and largely reversible relationship may seem to be in contrast with the hypothesis that the AGB's change with MAP is irreversible and bifurcation-induced (Staver et al., 2011; van Nes et al., 2014; Staal et al., 2020). However, this fact is not surprising, since our DGVM does not include land-atmosphere feedbacks such as moisture recycling. On the other hand, the biomass loss in the model is reversible in most regions even when enabling fire, which in previous works has been argued to be sufficient to give rise to alternative states under the same climatic conditions (Staver et al., 2011; Hirota et al., 2011), and which in fact can create alternative stable states in LPJmL when the model is coupled to an Earth system model (Drüke et al., 2023). The difference between the results by Drüke et al. (2023) and ours indicates that some land-atmosphere interactions may be necessary to obtain fire-induced alternative states. For example, the climate in a savanna is often hotter and drier than in a forest, and there can consequently be larger fire regimes in a savanna, which inhibit forest regrowth. Cells in the grassland state can start to grow trees on a larger scale if they receive sufficient precipitation and lower temperatures, or if they are close to cells with more favorable conditions and can get moisture by atmospheric transport. As a result, they can increase humidity and precipitation, and escape the fire trap (Oliveras and Malhi, 2016).

We find the existence of a threshold effect at a critical MAP value in vast parts of the Amazon Rainforest, with different potential sensitivity to reduced MAP for forests in different regions. Other studies employing the LPJ model have found similar nonlinear relationships or thresholds related to water availability, such as the dry season length (Levine et al., 2016; Cowling and Shin, 2006). It is also possible that some regions in the present-day Amazon are already in a regime of large AGB sensitivity even though the precipitation is still high. In our experiments, we could not detect a critical MAP value in some regions of the southern and eastern Amazon based on our Method (see Methods). Apart from the role of other limiting environmental properties that may affect the (non) linearity of the AGB response, a possible explanation for this lack of critical MAP is that the forest in these areas may have already entered a fast-response stage, and thus biomass in these regions is already relatively sensitive to changes in precipitation. One large fluctuation in precipitation or a few years of continuous decrease could then lead to large carbon losses.

Our results also indicate under which conditions certain factors dominate the critical MAP pattern. Most importantly, the critical MAP pattern is closely related to the seasonality of precipitation as measured by the SI (Fig. A7). We have also shown that the effect of seasonality persists when using aridity (PET divided by MAP) instead of MAP as the control variable (Fig. 5), which can account for spatial differences in potential evapotranspiration (Fig. 3).

In fact, PET can be interpreted as a separate explanatory variable that has an effect on critical MAP, since a larger evaporative demand requires higher rainfall values in order to maintain a certain soil moisture level, even for the same rainfall seasonality.

LPJmL computes PET by the Priestley-Taylor equation, which, in order to reduce dependency on observations, only relies on temperature and net radiation. Since temperature and the incoming radiative fluxes are prescribed, the only dynamic factor influencing PET is the surface albedo. Therefore, while forest cover remains high (which it does for MAP above the critical MAP), PET is constant in time. We can therefore treat PET as another background condition affecting critical MAP, with a certain spatial pattern but no time-dependence.

We therefore also examined the relationship between PET at the transition point and critical MAP (Supplementary Fig. A14), in addition to the relationship between seasonality and critical MAP (Supplementary Fig. A7 and A15). In our experiments, lower critical MAP corresponds to lower PET, as well as lower SI levels.

The estimation of partial correlation (see Methods) between critical MAP and SI excluding PET at the transition point exhibits partial correlations still >0.3 between critical MAP and SI patterns in the four model versions (Supplementary Fig. A15. Vice versa, when conditioning on SI, we find a substantial influence of PET (Supplementary Fig. A14). The results hence indicate that both SI and PET play a role in determining critical MAP.

It should be mentioned, however, that both explanatory variables are highly correlated (Fig. A16). Low PET and SI coincide in the central and western Amazon, and higher values occur in the south and east. We presume that in the north-western Amazon rainforest, precipitation exhibits little seasonality due to the Intertropical Convergence Zone (ITCZ) crossing twice a year, ensuring a regular and abundant supply of rainfall (Espinoza Villar et al., 2009). In addition, the increased cloud cover that comes with high precipitation limits solar radiation, leading to a relatively small PET (McAfee, 2013).

As shown in the previous section, fire disturbances and even more so variable root strategies have an impact on the vegetation biomass of the saturation state (where water ceases to be the limiting factor) in some areas. Upon the influence of variable root strategies, trees in parts of the eastern Amazon still retain more above-ground biomass before the equilibrium period approaches the transition, thereby decreasing the critical MAP threshold. The variable root strategy hence significantly increases the ability of trees to retain high biomass up to a smaller MAP threshold (e.g. Fig. A5). This result indicates that trees are developing adaptation strategies to dry conditions that may mediate their vulnerability to long-term changes in precipitation, which is in line with previous results (Ciemer et al., 2019; Smith and Boers, 2023a). In most parts of the Amazon, however, there is a high consistency in the non-linear relationship between AGB and MAP, regardless of whether or not the influences of a variable root strategy or wildfire disturbances are considered. In these regions, in particular in the western Amazon, variable-root strategies and fire disturbance have limited effects on critical MAP, with critical MAP patterns all maintaining similar behavior (Fig. A7 and A8).

In this context, the fact that variable root depth plays a role for critical MAP only in parts of the Amazon where seasonality and PET are high is suggestive. Where moisture availability is the same year-round, trees obtain no benefit in investing in deeper roots and storing water. In contrast, in the case of high SI, there is still a wet season without water limitation, but also a dry season, which leads to water storage in the deeper soil levels that deep roots can access during the dry season, thus gaining an advantage over plant types with shallow roots. Consequently, the same level of aridity (a constant property above critical MAP in our model setup) can allow for higher AGB levels when the roots are able to reach deep water (Fig. A5), and critical MAP is lower at some places in

the eastern Amazon when variable roots are considered (Fig. A8).

Regarding our result of critical slowing down (CSD) indicators, a significant number of cells show CSD before the critical MAP is reached, despite the fact that this threshold is not a discontinuous bifurcation point in the model and that the offline model setup does not include the land-atmosphere feedbacks that have previously been invoked to argue for a potential resilience loss of the Amazon rainforest (Zemp et al., 2017; Staal et al., 2020; Boulton et al., 2022; Boers et al., 2017; Bochow and Boers, 2023). Our results show that even this "stand-alone" forest can display dynamic CSD signals when approaching critical water stress, which raises the question what processes on what scales give rise to the CSD observed in the real world, as e.g. in (Boulton et al., 2022; Smith et al., 2022; Smith and Boers, 2023b). We argue that the increase in variance around the critical MAP value is straightforward to understand: When the sensitivity of AGB to MAP increases from essentially 0 to a substantially positive number, variations in MAP translate into increasing variations in AGB. In line with this explanation, the AGB variance decreases again once MAP is well below the critical value (not shown). In contrast, the behavior of autocorrelation is much harder to understand since the characteristic time scale of biomass fluctuations depends on a number of complex processes in the model. The most important processes involve the allocation of carbon to different pools, and the population dynamics of the different plant types, which are determined by a dynamic establishment, mortality, and the adjustment for area limitations (see Sitch et al. (2003)). The relevant processes behind this result should hence be further investigated in future studies. Interestingly, the autocorrelation increase is somewhat more widespread and stronger in model versions with variable deep roots (Fig. 6). The deep root version differs from the default model in several ways, in particular the introduction of two new carbon pools (root sapwood and root heartwood, i.e. slow pools compared to leaves and fine roots that have short turnover times), and the competition of many slightly different plant types, which may increase the typical time scale of population densities. It is therefore plausible that the differences between the model versions can be linked to these processes. In addition, the distribution of the CSD indicators shows a negative trend in variance and autocorrelation in some areas. At some grid cells, such as grid cell a in Fig. A17, where the CSD indicator decreases, the high MAP regime around 2000 mm/yr - 2500 mm/yr initially shows higher fluctuations in carbon pools, which is probably caused by competition between different plant types and results in a decrease in CSD indicators when MAP decreases. However, when MAP further decreases to around 2000 mm/yr, system stability can increase probably caused by adjustment of plant type composition. As the MAP continues to decline to around 1500 mm/yr, the local vegetation system again loses stability as it approaches the transition point (Fig. A17b). Therefore, the CSD indicator can show negative trends when assessed across the entirety of the MAP reduction process. Hence, it is possible that when the original MAP is large enough to allow more plant types to exist, the CSD indicator can show complex changes despite the monotonic decrease in MAP. An in-depth understanding of the process behind CSD indicators, vegetation plant types, and environmental conditions still requires further exploration.

Due to our idealized model setup, the full implications of our findings should be further analyzed in a climate-coupled model setting. Additionally, our focus is on the response of the vegetation system to precipitation changes under equilibrium or near-equilibrium conditions, and the impact of extreme events has not been taken into consideration. Both seasonality and extreme events are expected to increase with global warming (Seneviratne et al., 2021), so the true critical MAPs may be slightly larger, but the regional differences would remain. LPJmL enforces important bioclimatic limits and thresholds, at which mortality and growth can change dramatically when certain precipitation levels are reached (Cowling and Shin, 2006; Poulter et al., 2010). In this regard, the changes reflected in our experiments may potentially be more nonlinear than in the real world. However, given that the nonlinear relationship between biomass and rainfall we identify is only one branch of a feedback loop involving atmospheric processes like moisture recycling, we still see the possibility of rather abrupt losses in vegetation carbon in the real Amazon forest. Our results indicate that regions like the central Amazon, without pronounced seasonality and relatively small PET, will initially appear to persist even when drying, but may then suddenly lose larger amounts of carbon and trees, first because the drying affects all seasons, and second because the local tree types are not adapted to such dry conditions. Regions of the Amazon rainforest with smaller precipitation seasonality, such as the northwestern area, may hence face greater threats in a future drier climate.

Code availability

The model code used in this paper is available at doi:https://doi.org/10.5281/zenodo.10939988. The code used for the analysis are available on request from the corresponding author.

CRediT authorship contribution statement

Da Nian: Writing – review & editing, Writing – original draft, Visualization, Formal analysis, Conceptualization. **Sebastian Bathiany:** Writing – review & editing. **Boris Sakschewski:** Writing – review & editing, Investigation. **Markus Drüke:** Writing – review & editing, Investigation. **Lana Blaschke:** Writing – review & editing. **Maya Ben-Yami:** Writing – review & editing. **Werner von Bloh:** Software. **Niklas Boers:** Writing – review & editing, Supervision, Conceptualization.

Declaration of competing interest

The authors declare that they have no known competing financial interests or personal relationships that could have appeared to influence the work reported in this paper.

Data availability

All output data of LPJmL4.0-VR analyzed in this study can be found at doi:https://doi.org/10.5281/zenodo.8297598.

Amazon basin in this study is determined from (http://worldmap.harvard.edu/data/geonode:amapoly ivb). The precipitation and temperature dataset from CRU TS v. 4.06 can be downloaded at [https://catalogue.ceda.ac.uk/uuid/e0b4e1e56c1c4460b796073a31366980]. Other data sources used to operate and validate the LPJmL4.0 model versions in this research are detailed in the model description and evaluation paper Schaphoff et al. (2018a) and Schaphoff et al. (2018b).

Acknowledgments

This is ClimTip contribution #10; the ClimTip project has received funding from the European Union's Horizon Europe research and innovation programme under grant agreement No. 101137601. N.B. and S.B. acknowledge funding by the Volkswagen Foundation. M.D. acknowledges the project POEM-PBSim: A Simulator for Earth's Planetary Boundaries, funded by the Volkswagen Foundation at the Potsdam Institute for Climate Impact Research. B.S. acknowledges funding by Waldklimafonds in the project WaldSpektrum (2219WK39A4). M.B-Y. and N.B. have received funding from the European Union's Horizon 2020 research and innovation programme under the Marie Sklodowska-Curie grant agreement No. 956170.

Appendix A. Supplementary data

Supplementary data to this article can be found online at https://doi.org/10.1016/j.scitotenv.2024.174378.

References

Ahlström, A., Canadell, J.G., Schurgers, G., Wu, M., Berry, J.A., Guan, K., Jackson, R.B., 2017. Hydrologic resilience and Amazon productivity. Nature Communications 8 (1), 387. https://doi.org/10.1038/s41467-017-00306-z.

Armstrong McKay, D.I., Staal, A., Abrams, J.F., Winkelmann, R., Sakschewski, B., Loriani, S., Fetzer, I., Cornell, S.E., Rockström, J., Lenton, T.M., 2022. Exceeding 1.5 c global warming could trigger multiple climate tipping points. Science *377* (6611), eabn7950. https://doi.org/10.1126/science.abn7950.

Blaschke, L.L., Nian, D., Bathiany, Ben-Yami, M., Smith, T., Boulton, C.A., Boers, N., 2023. Spatial correlation increase in single-sensor satellite data reveals loss of Amazon rainforest resilience. arXiv. https://arxiv.org/abs/2310.18540[physics.geo-ph.

Bochow, N., Boers, N., 2023. The south american monsoon approaches a critical transition in response to deforestation. Science Advances 9 (40), eadd9973. https://doi.org/10.1126/sciadv.add9973.

Boers, N., 2021. Observation-based early-warning signals for a collapse of the Atlantic meridional overturning circulation. Nature Climate Change 11 (8), 680–688. https://doi.org/10.1038/s41558-021-01097-4.

Boers, N., Marwan, N., Barbosa, H.M., Kurths, J., 2017. A deforestationinduced tipping point for the South American monsoon system. Scientific Reports 7 (1), 41489. https://doi.org/10.1038/srep41489.

Boers, N., Ghil, M., Stocker, T.F., 2022. Theoretical and paleoclimatic evidence for abrupt transitions in the earth system. Environmental Research Letters 17 (9), 093006. https://doi.org/10.1088/1748-9326/ac8944.

Bondeau, A., Smith, P.C., Zaehle, S., Schaphoff, S., Lucht, W., Cramer, W., Gerten, D., Lotze-Campen, H., Müller, C., Reichstein, M., et al., 2007. Modelling the role of agriculture for the 20th century global terrestrial carbon balance. Global Change Biology 13 (3), 679–706. https://doi.org/10.1111/j.1365-2486.2006.01305.x.

Boulton, C.A., Lenton, T.M., Boers, N., 2022. Pronounced loss of Amazon rainforest resilience since the early 2000s. Nature Climate Change 12 (3), 271–278. https://doi.org/10.1038/s41558-022-01287-8.

Brauman, K.A., Freyberg, D.L., Daily, G.C., 2012. Potential evapotranspiration from forest and pasture in the tropics: A case study in kona, hawai ‘i. Journal of Hydrology 440, 52–61. https://doi.org/10.1016/j.jhydrol.2012.03.014.

Brovkin, V., Brook, E., Williams, J.W., Bathiany, S., Lenton, T.M., Barton, M., DeConto, R.M., Donges, J.F., Ganopolski, A., McManus, J., et al., 2021. Past abrupt changes, tipping points and cascading impacts in the earth system. Nature Geoscience 14 (8), 550–558. https://doi.org/10.1038/s41561-021-00790-5.

Bultan, S., Nabel, J.E., Hartung, K., Ganzenmüller, R., Xu, L., Saatchi, S., Pongratz, J., 2022. Tracking 21st century anthropogenic and natural carbon fluxes through model-data integration. Nature Communications 13 (1), 5516. https://doi.org/10.1038/s41467-022-32456-0.

Bush, M.B., 2017. The resilience of Amazonian forests. Nature 541 (7636), 167–168. https://doi.org/10.1038/541167a.

Buxton, J.E., Abrams, J.F., Boulton, C.A., Barlow, N., Rangel Smith, C., Van Stroud, S., Lees, K.J., Lenton, T.M., 2022. Quantitatively monitoring the resilience of patterned vegetation in the Sahel. Global Change Biology 28 (2), 571–587. https://doi.org/10.1111/gcb.15939.

Canadell, J.G., Monteiro, P., Costa, M., da Cunha, L.C., Cox, P., Eliseev, A., Henson, S., Ishii, S.J, M., et al., 2021. Global carbon and other biogeochemical cycles and feedbacks. In: Climate Change 2021: The Physical Science Basis. (Chapter in IPCC6). Cambridge University Press, United Kingdom and New York, USA.

Chou, C., Chiang, J.C., Lan, C.W., Chung, C.H., Liao, Y.C., Lee, C.J., 2013. Increase in the range between wet and dry season precipitation. Nature Geoscience 6 (4), 263–267. https://doi.org/10.1038/ngeo1744.

Christopher, E.D., Jenna, M.K., Benjamin, C.W., Camilo, R.S., Kelsey, R.C., Kali, B.M., Alexander, W.C., Michael, L.G., Humberto, R.D.R., Scott, D.M., Yadvinder, M., Sophie, F., Emanuel, G., Martijn, S., Imma, O.M., Kristine, Y.C., Gregory, R.G., Joshua, B.F., 2023. Tropical forests are approaching critical temperature thresholds. Nature 621, 105–111. https://doi.org/10.1038/s41586-023-06391-z.

Ciemer, C., Boers, N., Hirota, M., Kurths, J., Müller-Hansen, F., Oliveira, R.S., Winkelmann, R., 2019. Higher resilience to climatic disturbances in tropical vegetation exposed to more variable rainfall. Nature Geoscience 12 (3), 174–179. https://doi.org/10.1038/s41561-019-0312-z.

Ciemer, C., Winkelmann, R., Kurths, J., Boers, N., 2021. Impact of an AMOC weakening on the stability of the southern Amazon rainforest. European Physical Journal Special Topics 230 (14), 3065–3073. https://doi.org/10.1140/epjs/s11734-021-00186-x.

Cowling, S.A., Shin, Y., 2006. Simulated ecosystem threshold responses to co-varying temperature, precipitation and atmospheric CO2 within a region of Amazonia. Global Ecology and Biogeography 15 (6), 553–566. https://doi.org/10.1111/j.1466-8238.2006.00256.x.

Cox, P.M., Betts, R., Collins, M., Harris, P.P., Huntingford, C., Jones, C., 2004. Amazonian forest dieback under climate-carbon cycle projections for the 21st century. Theoretical and Applied Climatology 78, 137–156. https://doi.org/10.1007/s00704-004-0049-4.

Dakos, V., Kéfi, S., 2022. Ecological resilience: what to measure and how. Environmental Research Letters 17 (4), 043003. https://doi.org/10.1088/1748-9326/ac5767.

Dakos, V., Scheffer, M., Van Nes, E.H., Brovkin, V., Petoukhov, V., Held, H., 2008. Slowing down as an early warning signal for abrupt climate change. Proceedings of the National Academy of Sciences 105 (38), 14308–14312. https://doi.org/10.1073/pnas.0802430105.

Dijkstra, H.A., 2013. Nonlinear Climate Dynamics. Cambridge University Press.

Drijfhout, S., Bathiany, S., Beaulieu, C., Brovkin, V., Claussen, M., Huntingford, C., Scheffer, M., Sgubin, G., Swingedouw, D., 2015. Catalogue of abrupt shifts in intergovernmental panel on climate change climate models. Proceedings of the National Academy of Sciences 112 (43), E5777–E5786. https://doi.org/10.1073/pnas.1511451112.

Drüke, M., Forkel, M., Von Bloh, W., Sakschewski, B., Cardoso, M., Bustamante, M., Kurths, J., Thonicke, K., 2019. Improving the LPJmL4-SPITFIRE vegetation–fire model for South America using satellite data. Geoscientific Model Development 12 (12), 5029–5054. https://doi.org/10.5194/gmd-12-5029-2019.

Drüke, M., Bloh, W.V., Sakschewski, B., Wunderling, N., Petri, S., Cardoso, M., Barbosa, H.M., Thonicke, K., 2021a. Climate-induced hysteresis of the tropical forest in a fire-enabled earth system model. European Physical Journal Special Topics 230 (14), 3153–3162. https://doi.org/10.1140/epjs/s11734-021-00157-2.

Drüke, M., von Bloh, W., Petri, S., Sakschewski, B., Schaphoff, S., Forkel, M., Huiskamp, W., Feulner, G., Thonicke, K., 2021b. Cm2mc-lpjml v1. 0: biophysical coupling of a process-based dynamic vegetation model with managed land to a general circulation model. Geoscientific Model Development 14 (6), 4117–4141. https://doi.org/10.5194/gmd-14-4117-2021.

Drüke, M., Sakschewski, B., von Bloh, W., Billing, M., Lucht, W., Thonicke, K., 2023. Fire may prevent future Amazon forest recovery after large-scale deforestation. Communications Earth & Environment 4 (1), 248. https://doi.org/10.1038/s43247-023-00911-5.

Espinoza Villar, J.C., Ronchail, J., Guyot, J.L., Cochonneau, G., Naziano, F., Lavado, W., De Oliveira, E., Pombosa, R., Vauchel, P., 2009. Spatiotemporal rainfall variability in the Amazon basin countries (Brazil, Peru, Bolivia, Colombia, and Ecuador). International Journal of Climatology 29 (11), 1574–1594. https://doi.org/10.1002/joc.1791.

Flores, B.M., Montoya, E., Sakschewski, B., Nascimento, N., Staal, A., Betts, R.A., Levis, C., Lapola, D.M., Esqu'ıvel-Muelbert, A., Jakovac, C., et al., 2024. Critical transitions in the Amazon forest system. Nature 626 (7999), 555–564. https://doi.org/10.1038/s41586-023-06970-0.

Forkel, M., Drüke, M., Thurner, M., Dorigo, W., Schaphoff, S., Thonicke, K., von Bloh, W., Carvalhais, N., 2019. Constraining modelled global vegetation dynamics and carbon turnover using multiple satellite observations. Scientific Reports 9 (1), 18757. https://doi.org/10.1038/s41598-019-55187-7.

Fu, R., Yin, L., Li, W., Arias, P.A., Dickinson, R.E., Huang, L., Chakraborty, S., Fernandes, K., Liebmann, B., Fisher, R., et al., 2013. Increased dryseason length over southern Amazonia in recent decades and its implication for future climate projection. Proceedings of the National Academy of Sciences 110 (45), 18110–18115. https://doi.org/10.1073/pnas.1302584110.

Gerten, D., Schaphoff, S., Haberlandt, U., Lucht, W., Sitch, S., 2004. Terrestrial vegetation and water balance—hydrological evaluation of a dynamic global vegetation model. Journal of Hydrology 286 (1–4), 249–270. https://doi.org/10.1016/j.jhydrol.2003.09.029.

Gouttevin, I., Menegoz, M., Dominé, F., Krinner, G., Koven, C., Ciais, P., Tarnocai, C., Boike, J., 2012. How the insulating properties of snow affect soil carbon distribution in the continental pan-Arctic area. European Journal of Vascular and Endovascular Surgery 117 (G2). https://doi.org/10.1029/2011jg001916.

Harris, I., Osborn, T.J., Jones, P., Lister, D., 2020. Version 4 of the CRU TS monthly high-resolution gridded multivariate climate dataset. Scientific Data 7 (1), 109. https://doi.org/10.1038/s41597-020-0453-3.

Held, H., Kleinen, T., 2004. Detection of climate system bifurcations by degenerate fingerprinting. Geophysical Research Letters *31* (23). https://doi.org/10.1029/2004gl020972.

Hirota, M., Holmgren, M., Van Nes, E.H., Scheffer, M., 2011. Global resilience of tropical forest and savanna to critical transitions. Science 334 (6053), 232–235. https://doi.org/10.1126/science.1210657.

Holling, C.S., 1973. Resilience and stability of ecological systems. Annual Review of Ecology, Evolution, and Systematics 4 (1), 1–23. https://doi.org/10.1146/annurev.es.04.110173.000245.

Hutyra, L.R., Munger, J.W., Nobre, C.A., Saleska, S.R., Vieira, S.A., Wofsy, S.C., 2005. Climatic variability and vegetation vulnerability in Amazonia. Geophysical Research Letters 32 (24). https://doi.org/10.1029/2005gl024981.

Kéfi, S., Dakos, V., Scheffer, M., Van Nes, E.H., Rietkerk, M., 2013. Early warning signals also precede non-catastrophic transitions. Oikos 122 (5), 641–648. https://doi.org/10.1111/j.1600-0706.2012.20838.x.

Langenbrunner, B., Pritchard, M., Kooperman, G.J., Randerson, J.T., 2019. Why does Amazon precipitation decrease when tropical forests respond to increasing CO2? Earth's Future 7 (4), 450–468. https://doi.org/10.31223/osf.io/9fesz.

Lapola, D.M., Pinho, P., Barlow, J., Aragão, L.E., Berenguer, E., Carmenta, R., Liddy, H. M., Seixas, H., Silva, C.V., Silva-Junior, C.H., et al., 2023. The drivers and impacts of Amazon forest degradation. Science 379 (6630), eabp8622. https://doi.org/10.1126/science.abp8622.

Lasslop, G., Brovkin, V., Reick, C.H., Bathiany, S., Kloster, S., 2016. Multiple stable states of tree cover in a global land surface model due to a fire-vegetation feedback. Geophysical Research Letters 43 (12), 6324–6331. https://doi.org/10.1002/2016gl069365.

Lenton, T.M., 2011. Early warning of climate tipping points. Nature Climate Change 1 (4), 201–209. https://doi.org/10.1038/nclimate1143.

Lenton, T.M., Held, H., Kriegler, E., Hall, J.W., Lucht, W., Rahmstorf, S., Schellnhuber, H. J., 2008. Tipping elements in the Earth's climate system. Proceedings of the National Academy of Sciences 105 (6), 1786–1793. https://doi.org/10.1073/pnas.0705414105.

Lenton, T.M., Rockström, J., Gaffney, O., Rahmstorf, S., Richardson, K., Steffen, W., Schellnhuber, H.J., 2019. Climate tipping points—too risky to bet against. Nature 575 (7784), 592–595. https://doi.org/10.1038/d41586-019-03595-0.

Levine, N.M., Zhang, K., Longo, M., Baccini, A., Phillips, O.L., Lewis, S.L., Alvarez-D'avila, E., Segalin de Andrade, A.C., Brienen, R.J., Erwin, T.L., et al., 2016.

Ecosystem heterogeneity determines the ecological resilience of the Amazon to climate change. Proceedings of the National Academy of Sciences 113 (3), 793–797. https://doi.org/10.1073/pnas.1511344112.
Lovejoy, T.E., Nobre, C., 2018. Amazon tipping point. Science Advances 4 (2), eaat2340. https://doi.org/10.1126/sciadv.aat2340.
Lovejoy, T.E., Nobre, C., 2019. Amazon tipping point: last chance for action. Science Advances 5 (12), eaba2949. https://doi.org/10.1126/sciadv.aba2949.
Malhi, Y., Aragão, L.E., Galbraith, D., Huntingford, C., Fisher, R., Zelazowski, P., Sitch, S., McSweeney, C., Meir, P., 2009. Exploring the likelihood and mechanism of a climate-change-induced dieback of the Amazon rainforest. Proceedings of the National Academy of Sciences 106 (49), 20610–20615. https://doi.org/10.1073/pnas.0804619106.
MATLAB, T, 2021. Matlab version: 9.11.0.1809720 (r2021b).
McAfee, S.A., 2013. Methodological differences in projected potential evapotranspiration. Climatic Change 120, 915–930. https://doi.org/10.1007/s10584-013-0864-7.
Mitra, S.K., 2001. Digital Signal Processing: A Computer-Based Approach. McGraw-Hill Higher Education, New York, United States.
Nepstad, D.C., de Carvalho, C.R., Davidson, E.A., Jipp, P.H., Lefebvre, P.A., Negreiros, G. H., da Silva, E.D., Stone, T.A., Trumbore, S.E., Vieira, S., 1994. The role of deep roots in the hydrological and carbon cycles of Amazonian forests and pastures. Nature 372 (6507), 666–669. https://doi.org/10.1038/372666a0.
van Nes, E.H., Hirota, M., Holmgren, M., Scheffer, M., 2014. Tipping points in tropical tree cover: linking theory to data. Global Change Biology 20 (3), 1016–1021. https://doi.org/10.1111/gcb.12398.
Nian, D., Fu, Z., 2019. Extended self-similarity based multi-fractal detrended fluctuation analysis: A novel multi-fractal quantifying method. Communications in Nonlinear Science and Numerical Simulation 67, 568–576. https://doi.org/10.1016/j.cnsns.2018.07.034.
Pen~a-Claros, M., Poveda, G., Rodriguez, J., Saleska, S., Trumbore, S., Val, A., Villa Nova, L., Abramovay, R., Alencar, A., Rodr'ıguez Alzza, C., Armenteras, D., Artaxo, P., Athayde, S., Barretto Filho, H., Barlow, J., Berenguer, E., Bortolotto, F., Costa, F., Costa, M., Cuvi, N., Fearnside, P., Ferreira, J., Flores, B., Frieri, S., Gatti, L., Guayasamin, J., Hecht, S., Hirota, M., Hoorn, C., Josse, C., Lapola, D., Larrea, C., Larrea-Alcazar, D., Lehm Ardaya, Z., Malhi, Y., Marengo, J., Melack, J., Moraes, R., Moutinho, P., Murmis, M., Neves, E., Paez, B., Painter, L., Ramos, A., Rosero-Pen~a, M., Schmink, M., Sist, P., ter Steege, H., Val, P., van der Voort, H., Varese, M., Zapata R'ıos, G., 2021. In: Nobre, C., Encalada, A., Anderson, E., Roca Alcazar, F., Bustamante, M., Mena, C. (Eds.), Science Panel for the Amazon. Amazon Assessment Report 2021. United Nations Sustainable Development Solutions Network, New York, USA. Available from. https://www.theamazonwewant.org/amazon-assessment-report-2021/.
Oliveira, R., Bezerra, L., Davidson, E., Pinto, F., Klink, C., Nepstad, D., Moreira, A., 2005. Deep root function in soil water dynamics in cerrado savannas of Central Brazil. Functional Ecology 19 (4), 574–581. https://doi.org/10.1111/j.1365-2435.2005.01003.x.
Oliveras, I., Malhi, Y., 2016. Many shades of green: the dynamic tropical forest–savannah transition zones. Philosophical Transactions of the Royal Society B 371 (1703), 20150308. https://doi.org/10.1098/rstb.2015.0308.
Parry, I.M., Ritchie, P.D., Cox, P.M., 2022. Evidence of localised Amazon rainforest dieback in CMIP6 models. Earth System Dynamics 13 (4), 1667–1675. https://doi.org/10.5194/esd-13-1667-2022.
Pimm, S.L., 1984. The complexity and stability of ecosystems. Nature 307 (5949), 321–326. https://doi.org/10.1038/307321a0.
Poulter, B., Hattermann, F., Hawkins, E., Zaehle, S., Sitch, S., Restrepocoupe, N., Heyder, U., Cramer, W., 2010. Robust dynamics of Amazon dieback to climate change with perturbed ecosystem model parameters. Global Change Biology 16 (9), 2476–2495. https://doi.org/10.1111/j.1365-2486.2009.02157.x.
Richardson, T., Forster, P., Andrews, T., Boucher, O., Faluvegi, G., Fläschner, D., Kasoar, M., Kirkev°ag, A., Lamarque, J.F., Myhre, G., et al., 2018. Carbon dioxide physiological forcing dominates projected eastern Amazonian drying. Geophysical Research Letters 45 (6), 2815–2825. https://doi.org/10.1002/2017gl076520.
Sakschewski, B., Von Bloh, W., Drüke, M., Sörensson, A.A., Ruscica, R., Langerwisch, F., Billing, M., Bereswill, S., Hirota, M., Oliveira, R.S., et al., 2021. Variable tree rooting strategies are key for modelling the distribution, productivity and evapotranspiration of tropical evergreen forests. Biogeosciences 18 (13), 4091–4116. https://doi.org/10.5194/bg-18-4091-2021.
Schaphoff, S., Heyder, U., Ostberg, S., Gerten, D., Heinke, J., Lucht, W., 2013. Contribution of permafrost soils to the global carbon budget. Environmental Research Letters 8 (1), 014026. https://doi.org/10.1088/1748-9326/8/1/014026.
Schaphoff, S., Von Bloh, W., Rammig, A., Thonicke, K., Biemans, H., Forkel, M., Gerten, D., Heinke, J., Jägermeyr, J., Knauer, J., et al., 2018a. LPJmL4–a dynamic global vegetation model with managed land–part 1: model description. Geoscientific Model Development 11 (4), 1343–1375. https://doi.org/10.5194/gmd-11-1343-2018.
Schaphoff, S., Forkel, M., Müller, C., Knauer, J., Von Bloh, W., Gerten, D., Jägermeyr, J., Lucht, W., Rammig, A., Thonicke, K., Waha, K., 2018b. LPJmL4 – a dynamic global vegetation model with managed land – part 2: model evaluation. Geoscientific Model Development 11, 1377–1403. https://doi.org/10.5194/gmd-11-1377-2018.
Scheffer, M., Bascompte, J., Brock, W.A., Brovkin, V., Carpenter, S.R., Dakos, V., Held, H., Van Nes, E.H., Rietkerk, M., Sugihara, G., 2009. Earlywarning signals for critical transitions. Nature 461 (7260), 53–59. https://doi.org/10.5194/egusphere-egu21-2520.
Seneviratne, S., Zhang, X., Adnan, M., Badi, W., Dereczynski, C., Di Luca, A., Ghosh, S., Iskandar, I., Kossin, J., Lewis, S., et al., 2021. Weather and climate extreme events in a changing climate; climate change 2021: The physical science basis. In: Contribution of Working Group I to the Sixth Assessment Report of the Intergovernmental Panel on Climate Change (Chapter in IPCC6). Cambridge University Press, United Kingdom and New York, USA.
Signori-Müller, C., Oliveira, R.S., Barros, F.D.V., Tavares, J.V., Gilpin, M., Diniz, F.C., Zevallos, M.J.M., Yupayccana, C.A.S., Acosta, M., Bacca, J., et al., 2021. Non-structural carbohydrates mediate seasonal water stress across Amazon forests. Nature Communications 12 (1), 2310. https://doi.org/10.1038/s41467-021-22378-8.
Sitch, S., Smith, B., Prentice, I.C., Arneth, A., Bondeau, A., Cramer, W., Kaplan, J.O., Levis, S., Lucht, W., Sykes, M.T., et al., 2003. Evaluation of ecosystem dynamics, plant geography and terrestrial carbon cycling in the LPJ dynamic global vegetation model. Global Change Biology 9 (2), 161–185. https://doi.org/10.1046/j.1365-2486.2003.00569.x.
Sitch, S., Huntingford, C., Gedney, N., Levy, P., Lomas, M., Piao, S., Betts, R., Ciais, P., Cox, P., Friedlingstein, P., et al., 2008. Evaluation of the terrestrial carbon cycle, future plant geography and climate-carbon cycle feedbacks using five dynamic global vegetation models (DGVMs). Global Change Biology 14 (9), 2015–2039. https://doi.org/10.1111/j.1365-2486.2008.01626.x.
Smith, T., Boers, N., 2023a. Global vegetation resilience linked to water availability and variability. Nature Communications 14 (1), 498. https://doi.org/10.1038/s41467-023-36207-7.
Smith, T., Boers, N., 2023b. Reliability of vegetation resilience estimates depends on biomass density. Nature Ecology & Evolution 7, 1799–1808. https://doi.org/10.1038/s41559-023-02194-7.
Smith, T., Traxl, D., Boers, N., 2022. Empirical evidence for recent global shifts in vegetation resilience. Nature Climate Change 12 (5), 477–484. https://doi.org/10.1038/s41558-022-01352-2.
Smith, T., Zotta, R.M., Boulton, C.A., Lenton, T.M., Dorigo, W., Boers, N., 2023. Reliability of resilience estimation based on multi-instrument time series. Earth System Dynamics 14 (1), 173–183. https://doi.org/10.5194/esd-2022-41.
Staal, A., Fetzer, I., Wang-Erlandsson, L., Bosmans, J.H., Dekker, S.C., van Nes, E.H., Rockström, J., Tuinenburg, O.A., 2020. Hysteresis of tropical forests in the 21st century. Nature Communications 11 (1), 4978. https://doi.org/10.1038/s41467-020-18728-7.
Staver, A.C., Archibald, S., Levin, S.A., 2011. The global extent and determinants of savanna and forest as alternative biome states. Science 334 (6053), 230–232. https://doi.org/10.1126/science.1210465.
Thonicke, K., Spessa, A., Prentice, I., Harrison, S.P., Dong, L., CarmonaMoreno, C., 2010. The influence of vegetation, fire spread and fire behaviour on biomass burning and trace gas emissions: results from a processbased model. Biogeosciences 7 (6), 1991–2011. https://doi.org/10.5194/bgd-7-697-2010.
Tirabassi, G., Masoller, C., 2023. Entropy-based early detection of critical transitions in spatial vegetation fields. Proceedings of the National Academy of Sciences 120 (1), e2215667120. https://doi.org/10.1073/pnas.2215667120.
Valencia, S., Salazar, J.F., Hoyos, N., Armenteras, D., Villegas, J.C., 2024. Current forest–savanna transition in northern south america departs from typical climatic thresholds. Ecosystems 27, 61–76. https://doi.org/10.1007/s10021-023-00872-y.
Vatanen, T., Osmala, M., Raiko, T., Lagus, K., Sysi-Aho, M., Orešič, M., Honkela, T., Lähdesmäki, H., 2015. Self-organization and missing values in SOM and GTM. Neurocomputing 147, 60–70. https://doi.org/10.1016/j.neucom.2014.02.061.
Verbesselt, J., Umlauf, N., Hirota, M., Holmgren, M., Van Nes, E.H., Herold, M., Zeileis, A., Scheffer, M., 2016. Remotely sensed resilience of tropical forests. Nature Climate Change 6 (11), 1028–1031. https://doi.org/10.1038/nclimate3108.
Verweij, P., Schouten, M., Van Beukering, P., Triana, J., Van der Leeuw, K., Hess, S., et al., 2009. Keeping the Amazon forests standing: A matter of values. WWF-Netherlands. Available from. http://www.ivm.vu.nl/en/projects/Archive/keeping-the-amazon-standing/index.asp.
Walsh, R., Lawler, D., 1981. Rainfall seasonality: description, spatial patterns and change through time. Weather 36 (7), 201–208. https://doi.org/10.1002/j.1477-8696.1981.tb05400.x.
Wunderling, N., Donges, J.F., Kurths, J., Winkelmann, R., 2021a. Interacting tipping elements increase risk of climate domino effects under global warming. Earth System Dynamics 12 (2), 601–619. https://doi.org/10.5194/esd-2020-18.
Wunderling, N., Krönke, J., Wohlfarth, V., Kohler, J., Heitzig, J., Staal, A., Willner, S., Winkelmann, R., Donges, J.F., 2021b. Modelling nonlinear dynamics of interacting tipping elements on complex networks: the pycascades package. European Physical Journal Special Topics 230 (14–15), 3163–3176. https://doi.org/10.1140/epjs/s11734-021-00155-4.
Wunderling, N., Winkelmann, R., Rockström, J., Loriani, S., Armstrong McKay, D.I., Ritchie, P.D., Sakschewski, B., Donges, J.F., 2023. Global warming overshoots increase risks of climate tipping cascades in a network model. Nature Climate Change 13, 75–82. https://doi.org/10.1038/s41558-022-01545-9.
Zemp, D.C., Schleussner, C.F., Barbosa, H.M., Hirota, M., Montade, V., Sampaio, G., Staal, A., Wang-Erlandsson, L., Rammig, A., 2017. Selfamplified Amazon forest loss due to vegetation-atmosphere feedbacks. Nature Communications 8 (1), 14681. https://doi.org/10.1038/ncomms14681.